

# An Ultimate Investigation on the Adsorption of Amantadine on Pristine and Decorated Fullerenes $C_{59}X$ ( $X = Si, Ge, B, Al, Ga, N, P$ , and $As$ ): A DFT, NBO, and QTAIM Study

Mohsen Doust Mohammadi\*, Idris H. Salih† and Hewa Y. Abdullah†,‡

\*School of Chemistry, College of Science, University of Tehran, Tehran 14176, Iran

†Physics Education Department, Faculty of Education, Tishk International University, Erbil 44001, Iraq

‡Corresponding author. E-mail: hewayaseen@gmail.com

**ABSTRACT:** In this investigation, the feasibility of detecting the amantadine (AMD) molecule onto the outer surface of pristine fullerene ( $C_{60}$ ), as well as  $C_{59}X$  ( $X = Si, Ge, B, Al, Ga, N, P$ , and  $As$ ) decorated structures, was carefully evaluated. For achieving this goal, a density functional theory level of study using the HSEH1PBE functional together with a 6-311G(d) basis set has been used. Subsequently, the B3LYP-D3, wb97XD and M062X functionals with a 6-311G(d) basis set were also employed to consider the single point energies. Natural bond orbital (NBO) and the quantum theory of atoms in molecules (QTAIM) were implemented using the B3LYP-D3/6-311G(d) method and the results were compatible with the electronic properties. In this regard, the total density of states (TDOSS), the Wiberg bond index (WBI), natural charge, natural electron configuration, donor–acceptor NBO interactions, and the second-order perturbation energies are performed to explore the nature of the intermolecular interactions. All of the energy calculations and population analyses denote that by adsorbing of the AMD molecule onto the surface of the considered nanostructures, the intermolecular interactions are of the type of strong physical adsorption. Among the doped fullerenes, Ge-doped structure has very high adsorption energy compared to other elements. Generally, it was revealed that the sensitivity of the adsorption will be increased when the AMD molecule interacts with the decorated fullerenes and decrease the HOMO–LUMO band gap; therefore, the change of electronic properties can be used to design suitable nanocarrier.

**KEYWORDS:** Amantadine; fullerenes; AMD; density functional theory; natural bond orbital.

## 1. INTRODUCTION

The nano materials are structurally divided into carbon and noncarbon materials. After the discovery of fullerene in 1985 by Kroto *et al.* as a new carbon allotrope with unique features, scientists turned their attention to such structures.<sup>1–3</sup> Fullerene has shown amazing mechanical,<sup>4–7</sup> electromagnetic,<sup>8,9</sup> and chemical properties.<sup>10–12</sup> Using surface modification techniques, the properties of fullerenes can be significantly altered. For example, the solubility of fullerene, which is one of the basic properties in drug delivery, can be improved by functionalizing the surface.<sup>13–16</sup>

In the last two decades, theoretical studies in the density functional theory (DFT) framework on nanostructures have attracted the attention of many scientists in the fields of computational chemistry and

solid-state physics. The study of silicon carbide nanotube is no exception, and many theoretical studies on this nanostructure have led to interesting proposals for the manufacture of industrial devices. Theoretical studies show the molecular stability, structure, and properties of fullerene.<sup>17–20</sup> Heterofullerenes have also been widely studied: Xie *et al.* studied the sensor characteristic of  $C_{59}N^+$  and  $C_{48}N_{12}$ .<sup>21</sup> Matsubara and Massobrio performed a first-principle study on the silicon-doped fullerenes.<sup>22</sup> Haddon considered the superconductivity properties of alkali metal doped in  $C_{60}$ .<sup>23</sup> Fullerene and its derivatives are used in the

Received: 17 July 2020

Accepted: 21 September 2020

Published: 30 October 2020

absorption of many substances.<sup>18,24–30</sup> A brief study was performed by Alver *et al.* to investigate the interaction of amantadine (AMD) with C<sub>60</sub>.<sup>31</sup> The widespread use of silicon carbide nanotubes provides the basis for further study on such structures.

The AMD (also known as 1-amino-adamantine) drug molecule is the basis of many new drugs and chemicals. AMD was first discovered by Davis in 1964 and was used to treat the flu virus.<sup>32</sup> AMD is a member of the adamantane branch when an amino group joins one of the four most stable methine positions in adamantane to form C<sub>10</sub>H<sub>17</sub>N. This molecule is used in anti-viral drugs and in the treatment of Parkinson's and influenza A infections.<sup>33–36</sup> Although AMD is really cleared, there are some side effects that can be reduced using drug delivery methods like implementing carriers such as nanomaterial.<sup>37–39</sup>

This paper discusses the design of such a drug carrier. The main objective end of this study is to investigate the interactions of AMD with C<sub>60</sub> and C<sub>59</sub>X (X = Si, Ge, B, Al, Ga, N, P, and As) was studied. After optimizing the pristine and decorated fullerene structures by Gaussian software, to study the chemical stability and conductivity, the elements doping process on this fullerene have been studied. Because of the high sensitivity of computation to precisely determine the energy of molecular orbitals to investigate the conductivity and probability of physical and chemical adsorption, different structures need to be optimized using the appropriate computational methods. For this purpose, the HSEH1PBE functional and 6-311G(d) basis set was used in this research for computation. The B3LYP-D3, wB97XD and M062X functionals with a 6-311G (d) basis set were also used to calculate the single-point energies. Natural bond orbital (NBO) and quantum theory of atoms in molecules (QTAIM) were studied by using the HSEH1PBE/6-311G (d) method and the results were used to obtain various physical parameters.

## 2. COMPUTATIONAL DETAILS

The DFT calculations at HSEH1PBE functional together with 6-311G(d) Pople split-valence triple-zeta basis set with polarization functions<sup>40</sup> were used for geometry optimization for all different positions of the AMD/fullerene complex structures. To determine the stability of the optimized structures, frequency calculations are also performed using a similar level of theory to approve that all the stationary points are in agreement with a minimum point through the

potential energy surface. For further investigation, single-point energy calculations using different levels of theory were also applied to the most stable relaxed structures, which were obtained from geometry optimization at the HSEH1PBE/6-311G(d) level. The levels of theory used for the single point energy calculations included the B3LYP-D3, M06-2X, wB97XD together with 6-311G(d) basis set. NBO and the QTAIM were implemented by using the B3LYP-D3/6-311G(d) method. All the calculations including geometry optimization, single-point energy calculations and NBO analysis were performed by Gaussian 16 package.<sup>41</sup> It should be noted that the NBO calculations were performed using NBO v 3.0 software which is embedded within Gaussian software. In order to perform quantum theory of atoms in molecule (QTAIM) and density of state (DOS) analyses, the Multiwfn program.<sup>42–44</sup> was employed.

The adsorption energy ( $E_{\text{ads}}$ ) of the investigated AMD onto the surface of pristine and doped fullerenes can be calculated as follows:

$$E_{\text{ads}} = E_{\text{fullerene/CFM}} - (E_{\text{fullerene}} + E_{\text{AMD}}), \quad (1)$$

where  $E_{\text{fullerene/AMD}}$  represents the total energy of the complex structure.  $E_{\text{fullerene}}$  and  $E_{\text{AMD}}$  are the total energies of the pure fullerene and the pure AMD molecule, respectively. Note that the absorption energy consists of two parts, namely the interaction energy ( $E_{\text{int}}$ ) and the deformation energy ( $E_{\text{def}}$ ) that occur in the absorption process. Therefore, the following equations are used to calculate these proportions:

$$E_{\text{ads}} = E_{\text{int}} + E_{\text{def}}, \quad (2)$$

$$\begin{aligned} E_{\text{int}} &= E_{\text{fullerene/CFM}} - E_{\text{fullereneincomplex}} \\ &\quad - E_{\text{AMDincomplex}}, \end{aligned} \quad (3)$$

$$\begin{aligned} E_{\text{def}} &= E_{\text{def}}^{\text{fullerene}} + E_{\text{def}}^{\text{AMD}} \\ &= (E_{\text{fullereneincomplex}} - E_{\text{pristinefullerene}}) \\ &\quad + (E_{\text{AMDincomplex}} - E_{\text{isolatedAMD}}), \end{aligned} \quad (4)$$

where  $E_{\text{fullereneincomplex}}$  and  $E_{\text{AMDincomplex}}$  are energies of AMD molecule and fullerene in the optimized complexes, respectively.

## 3. RESULT AND DISCUSSION

### 3.1. The structural analysis

To optimize the structure of pristine fullerene structure using the DFT method, we selected HSEH1PBE functional together with basis set 6-311G (d). After

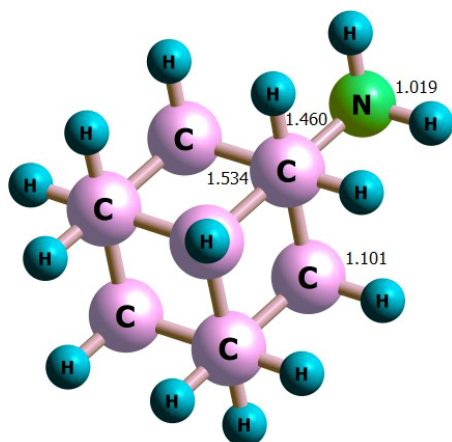


**Fig. 1.** The geometry information of the AMD molecule. The optimization process has been done using HSEH1PBE/6-311G (d) level of theory. The atomic distances are expressed in Angstrom ( $\text{\AA}$ ).

optimization of the pristine  $C_{60}$  we substituted a carbon atom with  $X$  ( $X = \text{Si}, \text{Ge}, \text{B}, \text{Al}, \text{Ga}, \text{N}, \text{P}$ , and  $\text{As}$ ) elements then the optimization process has been repeated for doped structures. Figure 1 shows the structure of AMD and quantitative values of bond lengths for isolated  $C_{60}$  are shown in Fig. 2. Figures S1–S8 show the values of bond lengths for other isolated cages in the supplementary material.

The next step was the optimization of AMD with  $C_{60}$  as well as  $C_{59}X$  complexes. In this step, the AMD molecule was placed on the outer surface of each

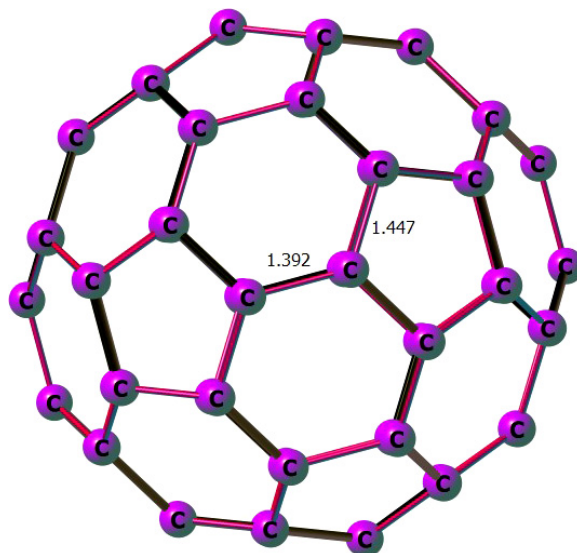


**Fig. 2.** The values of bond length for  $C_{60}$ . The optimization process has been done using HSEH1PBE/6-311G (d) level of theory. The atomic distances are expressed in Angstrom ( $\text{\AA}$ ).

above-mentioned structures with a vertical distance of about 2.1  $\text{\AA}$ . To find out the optimum distances between fullerene and AMD molecules, we used the rigid scan for some cases to estimate the most efficient distance. It should be noted that the level of theory in both optimization and the rigid scan was HSEH1PBE/6-311G (d). To better explain the details of the adsorption process, it will be useful to compare Figs. 2 and 3. In addition, Figs. S9–S16 show the most stable form of  $\text{AMD}/\text{C}_{59}\text{X}$ ,  $X = \text{Si}, \text{Ge}, \text{B}, \text{Al}, \text{Ga}, \text{N}, \text{P}$ , and  $\text{As}$ ) in the supplementary material.

The fullerene is composed of several symmetric hexagons and pentagons that have five different adsorption positions for the adsorption of any molecule onto the outer surface shown in Fig. 4: adsorption position on the carbon atom ( $T_1$ ), between two hexagonal rings ( $T_2$ ), between two hexagonal and pentagonal rings ( $T_3$ ), adsorption position at the hexagonal center ( $T_4$ ), and adsorption position at the pentagonal center ( $T_5$ ). The logical approach is to put the AMD molecule in each of these positions and measure the amount of adsorption energy ( $E_{\text{ads}}$ ). It is important to note that the AMD molecule has different heads (H, N), and each of these heads must be placed on the desired position on the fullerene to measure the amount of absorption energy. Our experience shows that negligible differences exist in the amounts of adsorption energies when we place the AMD in any of the possible adsorption sites. As mentioned in Ref. 45, when the differences in the adsorption energies are “below the range of chemical interest”, placing the AMD in different positions on the fullerene provides identical results. Nevertheless, we put the AMD molecule from N-head onto the desired positions on the outer surface of fullerene structures. The test result showed that there is a negligible difference among the adsorption energies; therefore, the center of the hexagonal ring position was the target position on the fullerene.

Single point energy calculations using different functional such as B3LYP-D3, wB97XD and M062X with a 6-311G (d) basis set were done. The calculated values indicate strong interactions between fullerenes and AMD molecule. Since the HSEH1PBE functional does not account for the scattering contribution, it is expected that in poor interactions, this functional will not give a good estimate of the amount of energy. For this reason, methods have been developed for long-range and dispersion effects. In this work, we used B3LYP-D3 and wB97XD to consider long range and dispersion effects. The well-known M062X functional is used for better comparison. The results show that the

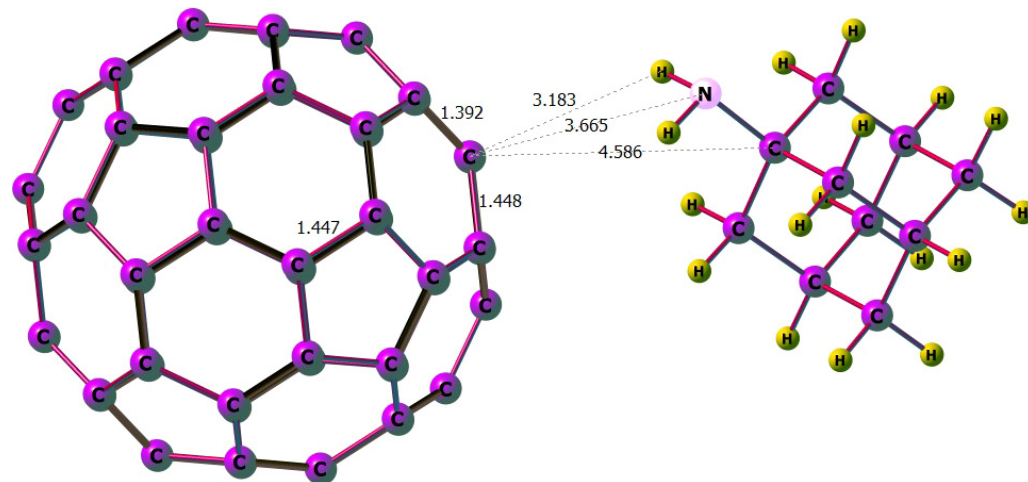


**Fig. 3.** The most stable form of AMD/C<sub>60</sub>. The cluster has been optimized using the HSEH1PBE functional and 6-311G(d) basis set. The atomic distances are expressed in Angstrom (Å).

energies obtained from the HSEH1PBE and other functionals are consistent with the accuracy of the calculations. On the other hand, as expected, the B3LYP-D3 method shows higher values of energy than the others, due to the dispersion contribution consideration. Also, by doping the Al and Ga elements on the fullerene, significant changes in the results are achieved. Table 1 shows that doping Al and Ga increases the absorption energy and enhanced chemical absorption. The related deformation energies ( $E_{\text{def}}$ ) are reported in Table S1 in the supplementary material. Table 2 also shows the bond length and the nearest intermolecular

distances (re(Å)) between AMD molecule and C<sub>60</sub> as well as C<sub>59</sub>X.

### 3.2. Energetics properties

The chemical electron potential ( $\mu$ ) describes the tendency of electrons to escape from a particular species at the ground state. This quantity is equal to the absolute negative electronegativity obtained from the definition provided by Mulliken, as follows:

$$\mu = -xM. \quad (5)$$

Parr and his colleagues<sup>46</sup> used the DFT to show that at a constant external potential, the potential energy of an electron is related to the first derivative of energy relative to the number of electrons, as follows:

$$\mu = \left( \frac{\partial E}{\partial N} \right)_{v(r)} = -\frac{1}{2} (\text{IP} + \text{EA}), \quad (6)$$

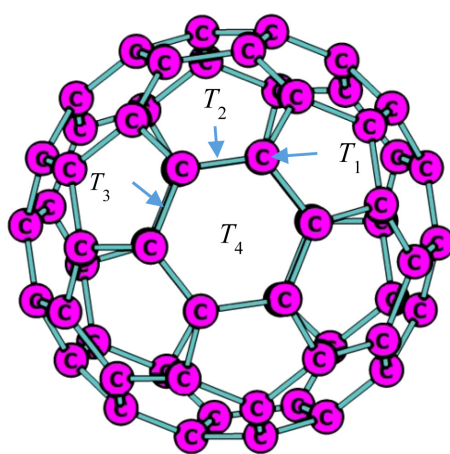


**Fig. 4.** All possible target positions for the adsorption of any arbitrary molecules onto the surface fullerene. Top of carbon atom (T<sub>1</sub>), between two hexagonal rings (T<sub>2</sub>), between hexagonal and pentagonal rings (T<sub>3</sub>), top of the hexagonal ring (T<sub>4</sub>), and top of the pentagonal ring (T<sub>5</sub>).

**Table 1.** The adsorption energies ( $E_{\text{ads}}$ ) for pristine C<sub>60</sub> and C<sub>59</sub>X (X = Si, Ge, B, Al, Ga, N, P, and As) with AMD molecule. All values are in (eV).

System	HSEH1PBE	B3LYP-D3	M06-2X	wB97XD
AMD/C <sub>60</sub>	-0.056	-0.128	-0.111	-0.213
AMD/C <sub>59</sub> Si	-1.650	-1.786	-1.945	-2.015
AMD/C <sub>59</sub> Ge	-1.730	-1.791	-2.173	-2.091
AMD/C <sub>59</sub> B	-0.068	-0.255	-0.129	-0.252
AMD/C <sub>59</sub> Al	-2.227	-2.463	-2.451	-2.511
AMD/C <sub>59</sub> Ga	-2.196	-2.414	-2.447	-2.526
AMD/C <sub>59</sub> N	-0.058	-0.237	-0.116	-0.238
AMD/C <sub>59</sub> P	-0.078	-0.265	-0.153	-0.251
AMD/C <sub>59</sub> As	-0.424	-0.713	-0.568	-0.684

**Table 2. The bond lengths and the nearest intermolecular distances ( $r_e$  (Å)) between AMD molecule with pristine  $C_{60}$  and  $C_{59}X$  ( $X = Si, Ge, B, Al, Ga, N, P, and As$ ). All calculations were performed using PBC-DFT HSEH1PBE/6-311G (d) level of theory.**

Systems	N... (x)	H... (x)	C... (x)	C-C	C-(x)
$C_{60}$	—	—	—	1.447	1.392
$C_{59}Si$	—	—	—	1.447	1.837
$C_{59}Ge$	—	—	—	1.447	1.908
$C_{59}B$	—	—	—	1.453	1.545
$C_{59}Al$	—	—	—	1.435	1.900
$C_{59}Ga$	—	—	—	1.436	1.906
$C_{59}N$	—	—	—	1.451	1.399
$C_{59}P$	—	—	—	1.455	1.829
$C_{59}As$	—	—	—	1.440	1.902
AMD/ $C_{60}$	3.665	3.183	4.586	1.447	1.392
AMD/ $C_{59}Si$	1.933	2.453	3.006	1.448	1.774
AMD/ $C_{59}Ge$	2.015	2.523	3.044	1.434	1.826
AMD/ $C_{59}B$	5.827	4.861	6.493	1.442	1.524
AMD/ $C_{59}Al$	2.013	2.487	3.041	1.392	1.938
AMD/ $C_{59}Ga$	2.027	2.519	3.010	1.446	1.941
AMD/ $C_{59}N$	4.164	4.631	4.637	1.449	1.401
AMD/ $C_{59}P$	3.957	3.366	4.593	1.446	1.829
AMD/ $C_{59}As$	4.130	3.289	4.070	1.392	1.935

where IP and EA are the ionization affinity and electron affinity, respectively.<sup>47</sup> Based on the Koopman approximation (see the Hartree–Fock theory) and Janak's approximation,<sup>48</sup> the chemical potential is defined as follows:

$$\mu = \left( \frac{\partial E}{\partial N} \right)_{v(r)} \approx \frac{(\varepsilon_{LUMO} + \varepsilon_{HOMO})}{2}, \quad (7)$$

where  $\varepsilon_{HOMO}$  and  $\varepsilon_{LUMO}$  are the energies of the HOMO and the LUMO, respectively.  $N$  is the number of electrons,  $E$  is the total electronic energy of the system and  $v(r)$  is the external potential.

Comparison of the variation in electron chemical potentials to that in the number of electrons at a constant external potential is called chemical hardness, which is expressed as follows:

$$\eta = \left( \frac{\partial \mu}{\partial N} \right) = \frac{1}{2} \left( \frac{\partial^2 E}{\partial N^2} \right). \quad (8)$$

Parr *et al.*<sup>49</sup> used the electron energy curve as well as the finite difference approximation to express hardness as follows:

$$\eta = \frac{1}{2} (IP - EA). \quad (9)$$

Moreover, using Janak and Koopman's approximations, the hardness equation is transformed as follows:

$$\Delta E_{min} = -\frac{\mu^2}{2\eta}. \quad (10)$$

Chemical hardness is the energy gap between the HOMO and the LUMO. Therefore, molecules with high energies are considered as hard molecules, while those with low energies are called soft molecules. Since the softness of a molecule is the opposite of its hardness, the equation for molecule softness is denoted as follows<sup>50</sup>:

$$S = \frac{1}{\eta}. \quad (11)$$

Inspired by Maynard's work, Parr *et al.*<sup>51</sup> introduced electrophilicity as the steady-state energy in which an atom or a molecule at ground state gains by receiving additional electron charges from the environment. The energy changes that lead to such a charge transfer are expressed as follows:

$$\Delta E = \mu \Delta N + \frac{1}{2} \eta (\Delta N)^2. \quad (12)$$

When the system receives electron charges from the environment sufficient to equate its potential to that of the environment, the system is saturated with electrons and can be expressed as follows:

$$\frac{d\Delta E}{d\Delta N} = 0. \quad (13)$$

The electron load received from the environment is maximized, and the total energy of the system is eventually minimized. Thus,

$$\Delta N_{max} = -\frac{\mu}{\eta}, \quad (14)$$

$$\Delta E_{min} = -\frac{\mu^2}{2\eta}. \quad (15)$$

Since  $\eta > 0$ ,  $\Delta E < 0$  always, and the charge transfer is energetically desirable. Accordingly, Parr *et al.* proposed the following equation to denote the electrophilicity of electrophilic species.

$$\omega = \frac{\mu^2}{2\eta}. \quad (16)$$

In fact, the electrophilicity index is the capacity of a species to accept an arbitrary number of electrons from the environment.<sup>52</sup>

**Table 3.** Values of HOMO energy ( $\varepsilon_H$ ), LUMO energy ( $\varepsilon_L$ ), HOMO and LUMO energy gap (HLG), chemical potential ( $\mu$ ), chemical hardness ( $\eta$ ), and electrophilicity ( $\omega$ ). All values are in (eV) and were obtained from completed fullerene B3LYP-D3/6-311G (d) level of theory.

System	$\varepsilon_H$	$\varepsilon_L$	HLG	$\mu$	$\eta$	$\omega$
$C_{60}$	-5.974	-3.212	2.763	-4.593	1.381	14.569
$C_{59}Si$	-5.794	-3.617	2.177	-4.705	1.089	12.050
$C_{59}Ge$	-5.856	-3.726	2.130	-4.791	1.065	12.221
$C_{59}B$	-5.645	-3.210	2.435	-4.428	1.217	11.933
$C_{59}Al$	-5.366	-3.097	2.269	-4.231	1.134	10.154
$C_{59}Ga$	-5.433	-3.185	2.249	-4.309	1.124	10.438
$C_{59}N$	-4.559	-3.281	1.278	-3.920	0.639	4.908
$C_{59}P$	-5.176	-3.239	1.938	-4.208	0.969	8.576
$C_{59}As$	-5.221	-3.209	2.012	-4.215	1.006	8.939
AMD/ $C_{60}$	-6.017	-3.277	2.740	-4.647	1.370	14.789
AMD/ $C_{59}Si$	-4.610	-2.537	2.073	-3.574	1.037	6.619
AMD/ $C_{59}Ge$	-4.602	-2.551	2.051	-3.576	1.025	6.557
AMD/ $C_{59}B$	-5.710	-3.271	2.439	-4.491	1.219	12.295
AMD/ $C_{59}Al$	-4.698	-2.559	2.140	-3.628	1.070	7.043
AMD/ $C_{59}Ga$	-4.711	-2.601	2.110	-3.656	1.055	7.049
AMD/ $C_{59}N$	-4.633	-3.339	1.294	-3.986	0.647	5.139
AMD/ $C_{59}P$	-5.227	-3.284	1.943	-4.256	0.972	8.799
AMD/ $C_{59}As$	-5.275	-3.248	2.027	-4.261	1.013	9.200

The values of maximum occupied molecular orbital (HOMO) and lowest occupied atomic orbital (LUMO) and their differences (HLG), chemical potential ( $\mu$ ), chemical hardness ( $\eta$ ), and electrophilicity ( $\omega$ ) are reported in Table 3. From the results of this table, it can be seen that by adsorption of AMD molecule, the

distance between HOMO and LUMO levels is reduced relative to the pure fullerene. Dopping Ga element shows the greatest decrease in the interaction of the fullerene structures and AMD, which is caused by the molecular energy absorption matched from this position. The decrease in HLG results in an increase in the electrical conductivity and thus an increase in the metal property of all the  $C_{59}X$  compared to pure  $C_{60}$ . It is also noteworthy that the observed changes in HLG after doped Al and Ga are mainly due to lower LUMO energy levels. To study these changes in the electron structure of the studied cases more closely, the density of state spectra (DOS) will be analyzed in Sec. 3.3. For a more detailed study of the electron structure changes, the density of state spectra (DOS) diagrams for isolated  $C_{60}$  and AMD/ $C_{60}$  cluster are extracted and illustrated in Figs. 5 and 6. Moreover, the DOS diagrams for other systems are shown through S17–S32 in the supplementary material.

From the DOS spectra, it is clear that DOS spectra for all absorption are in agreement with the values of the energy parameters reported in Table 3. The lowest amount of adsorption energy is related to the pristine fullerene and the highest amount of adsorption energy is for the adsorption of AMD onto the Ga-doped fullerene, the most changes are also observed in the DOS spectrum relative to this structure. In other words, the electron structure changes show a direct relationship with the absorption energies. Given the amount of absorption energy, high amount of binding energy, and the structure of DOS spectra obtained in all of these

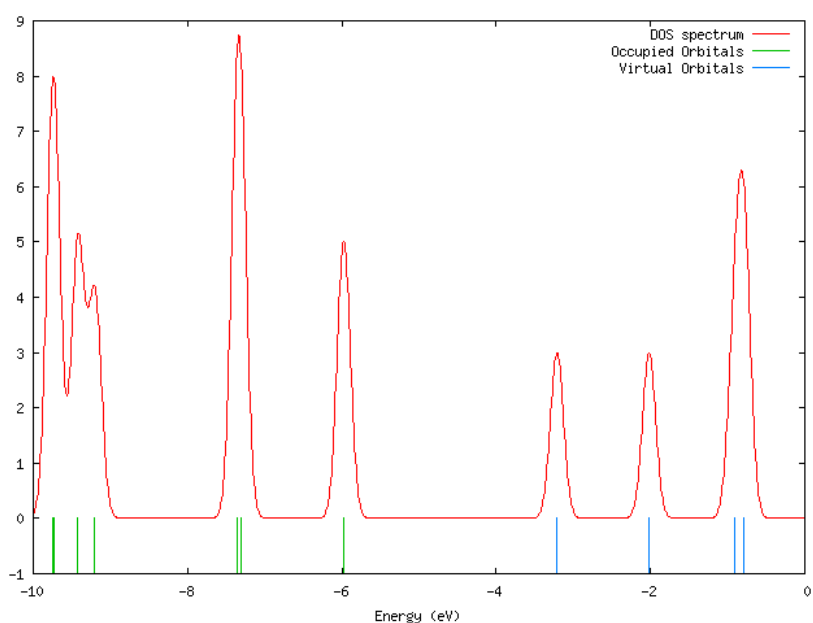


**Fig. 5.** The density of state (DOS) diagram for the  $C_{60}$ . The data were obtained from B3LYP-D3/6-311G (d) level of theory.

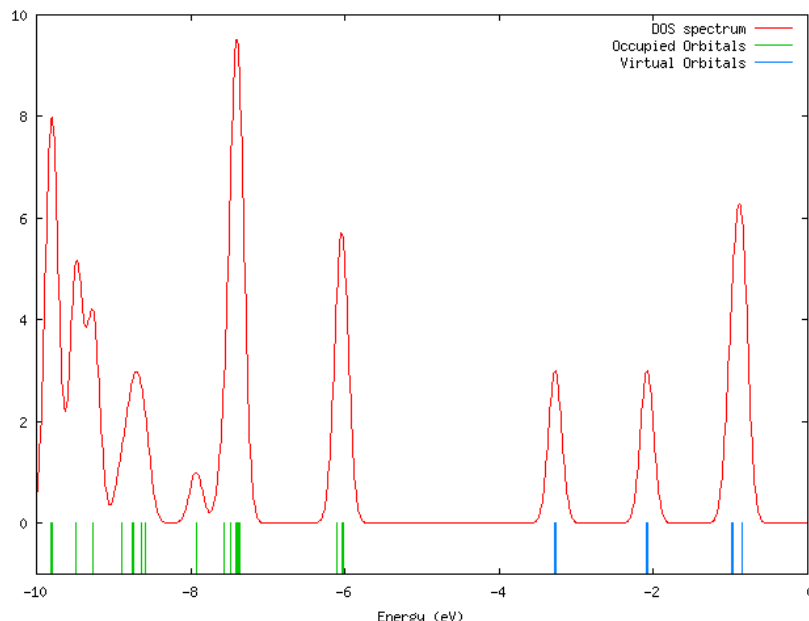


**Fig. 6.** The density of state (DOS) diagram for the adsorption of AMD molecule onto the surface of the  $C_{60}$ . The data were obtained from B3LYP-D3/6-311G (d) level of theory.

cases, it can be claimed that the adsorptions of AMD molecule onto  $C_{60}$  and  $C_{59}X$  structures are a strong physical adsorption type.

### 3.3. NBO and QTAIM analyses

In the NBO approach,<sup>53,54</sup> a given wave function should be transformed into a localized form in which NBOs are considered as local block eigenfunctions of the density matrix. NBO analysis is applicable in both closed-shell and open-shell systems which are calculated from atom-centered basis functions.<sup>55</sup> Second-order perturbation theory is also one of the highest used methods for estimating energy effects.<sup>56–66</sup>

We used the B3LYP-D3/6-311g(d) level of theory to perform the NBO calculations. The concept of bonded orbitals can be used to understand the distribution of electrons in atomic and molecular orbitals. NBO is defined as the following equation for  $\sigma$  bonding between atoms A and B.

$$\sigma_{AB} = C_A h_A + C_B h_B, \quad (17)$$

where  $h_A$  and  $h_B$  are natural hybrids on the A and B atoms. In the covalent limit,  $C_A = C_B$ , and at the ionic limit,  $C_A \gg C_B$  (if the electronegativity of A is greater than B). Each bonding NBO must be paired with a corresponding anti-bonding NBO.

$$\sigma_{AB}^* = C_A h_A - C_B h_B. \quad (18)$$

In NBO analysis, molecular energy is divided into two parts: total energy (for nonstationary enters) and Lewis molecule energy (where super-conjugation does not occur, and the electrons are strongly bound in single bonds and pairs). The occupied NBOs describe the covalent effects in the molecule, while the nonoccupied NBOs are used to describe noncovalent effects. The most important nonoccupied NBOs are anti-bond orbitals.<sup>53,65,66</sup>

Various types of bond order analyses are developed to take into account the bond property such as Mulliken bond order analysis,<sup>67</sup> Mayer bond order analysis,<sup>68,69</sup> Multi-center bond order analysis,<sup>70,71</sup> Wiberg bond order analysis,<sup>72</sup> Fuzzy bond order<sup>73,74</sup> and so on. Due to the different assumptions, caution should be exercised when using the above-mentioned methods for example basis set containing diffuse functions as case in point, leads to unreliable results for Mulliken or Mayer analyses.<sup>42</sup>

According to the literature,<sup>75</sup> the Wiberg bond order, in comparison to the Mayer method, has much less sensitivity to the basis set. The WBI is the sum of squares of off-diagonal density matrix elements between atoms and is denoted as follows:

$$\text{WBI} = \sum_k p_{jk}^2 = 2p_{jj} - p_{jj}^2, \quad (19)$$

where  $P_{jk}$  represents the density matrix elements (i.e. the contribution of interactions between basis functions

$j$  and  $k$ ) and  $P_{jj}$  is the charge density in the atomic orbital. In the WBI, there is no difference between net bonding or anti-bonding type of elements of the density matrix.

NBO analysis was used to calculate the bond order using the Wiberg method,<sup>72</sup> for a more detailed examination of the types of interactions. After studying the adsorption energy of the complexes, we examine the bond length and bond order of the AMD and fullerenes before and after the adsorption. The Wiberg bond order for these clusters is reported in Table S2. According to this table, the bonds of the nitrogen atoms in AMD molecules oriented to the  $X$  ( $X = \text{Si, Ge, B, Al, Ga, N, P, and As}$ ) atom in  $\text{C}_{59}\text{X}$  are the most significant bonds. The results of the WBI analysis agree with the adsorption energies, as reported in Table 1. They reveal that these fullerenes show a strong interaction with the AMD molecules and can be considered a suitable drug carrier for it.

The results of the NBO calculations shed light on the natural electron configuration and partial natural charge, which are useful in the study of the character of the bond between the AMD and the fullerenes. The NBO approach was implemented for all atoms in the pristine and cluster systems to reveal the quantities listed in Table 4. Charge transfer quantity between AMD molecule and fullerenes can also be a criterion to study the interaction of fullerene and AMD, such that the stronger the interaction, the more the charge transfer between AMD and the fullerene. Table 4 shows that there is a significant charge transfer between two species during the adsorption process would happen.

In addition, by implementing the natural electron configuration, the type of interaction between fullerenes and AMD molecules will be described. From Table 4, it can be obvious that valance configuration of isolated AMD molecule and fullerenes, as well as valance configuration of fullerene/AMD clusters, have been increased. Therefore, the interaction of AMD with  $\text{C}_{60}$  and  $\text{C}_{59}\text{X}$  can be classified as a strong physical adsorption process.

The second-order perturbation theory estimate of donor–acceptor interactions in the NBO basis. For each donor NBO ( $i$ ) and acceptor NBO ( $j$ ), the stabilization energy  $E(2)$  is calculated as follows<sup>63</sup>:

$$E(2) = \Delta E_{ij}^2 = -q_i \frac{(F_{ij})^2}{(\varepsilon_j - \varepsilon_i)}, \quad (20)$$

where  $\varepsilon_i$ ,  $\varepsilon_j$  are diagonal elements which show the orbital energies,  $q_i$  denotes the donor orbital occupancy ( $q = 2$  for closed-shell systems and  $q = 1$

**Table 4.** Natural electron configurations and natural charges (esu) for the isolated AMD, pristine  $\text{C}_{60}$  and  $\text{C}_{59}\text{X}$  ( $X = \text{Si, Ge, B, Al, Ga, N, P, and As}$ ) and their complex structures. All values calculated by the B3LYP-D3/6-311G(d) level of theory.

Systems	Atom	Natural charge	Natural electron configuration
$\text{C}_{60}$	C	0.000	[core]2S (0.87)2p(3.12)3p(0.01)
$\text{C}_{59}\text{Si}$	C	-0.003	[core]2S (0.87)2p(3.12)3p (0.01)
	Si	1.306	[core]3S (0.98)3p(1.69)3d(0.02)4p (0.01)
$\text{C}_{59}\text{Ge}$	C	-0.005	[core]2S (0.87)2p(3.12)3p(0.01)
	Ge	1.100	[core]4S (1.17)4p(1.73)4d(0.01)5p (0.01)
$\text{C}_{59}\text{B}$	C	-0.001	[core]2S (0.87)2p(3.12)3p(0.01)
	B	0.707	[core]2S (0.60)2p(1.68)3p(0.01)
$\text{C}_{59}\text{Al}$	C	-0.002	[core]2S (0.86)2p(3.12)3p(0.01)
	Al	1.642	[core]3S (0.65)3p(0.70)3d(0.01)4p (0.01)
$\text{C}_{59}\text{Ga}$	C	-0.002	[core]4S (0.78)4p(0.85)4d(0.01)
	Ga	1.391	[core]4S (0.78)4p(0.85)4d(0.01)
$\text{C}_{59}\text{N}$	C	-0.003	[core]2S (0.87)2p(3.12)3p(0.01)
	N	-0.345	[core]2S (1.18)2p(4.15)3p(0.01)
$\text{C}_{59}\text{P}$	C	-0.001	[core]2S (0.85)2p(3.12)3p(0.01)
	P	1.037	[core]4S (1.41)4p(2.01)4d(0.01)5p (0.01)
$\text{C}_{59}\text{As}$	C	-0.001	[core]2S (0.86)2p(3.12)3p(0.01)
	As	1.022	[core]4S (1.52)4p(2.44)4d(0.01)5p (0.01)
$\text{AMD/C}_{60}$	C	0.001	[core]2S (0.87)2p(3.12)3p(0.01)
	N	-0.886	[core]2S (1.42)2p(4.45)3p(0.01)3d (0.01)
	C	0.135	[core]2S (0.87)2p(2.98)3p(0.01)3d (0.01)
	H	0.370	1S (0.63)
$\text{AMD/C}_{59}\text{Si}$	C	0.001	[core]2S (0.87)2p(3.12)3p(0.01)
	Si	1.920	[core]3S (0.72)3p(1.32)3d(0.03)4p (0.01)
	N	-0.940	[core]2S (1.41)2p(4.51)3p(0.01)
	C	-0.464	[core]2S (0.89)2p(2.95)3p(0.01)
$\text{AMD/C}_{59}\text{Ge}$	H	0.448	1S (0.55)
	C	0.001	[core]2S (0.87)2p(3.12)3p(0.01)
	Ge	1.719	[core]4S (0.88)4p(1.40)4d(0.01)5p (0.01)
	N	-0.898	[core]2S (1.40)2p(4.48)3p(0.01)
$\text{AMD/C}_{59}\text{B}$	C	-0.027	[core]2S (0.88)2p(2.96)3p(0.01)
	H	0.446	1S (0.55)
	C	0.001	[core]2S (0.87)2p(3.12)3p(0.01)
	B	0.707	[core]2S (0.60)2p(1.68)3p(0.01)
$\text{AMD/C}_{59}\text{Al}$	N	-0.886	[core]2S (1.42)2p(4.45)3p(0.01)3d (0.01)
	C	0.136	[core]2S (0.87)2p(2.98)3p(0.01)3d (0.01)
	H	0.368	1S (0.63)
	C	0.001	[core]2S (0.87)2p(3.12)3p(0.01)
$\text{AMD/C}_{59}\text{Al}$	Al	1.703	[core]3S (0.53)3p(0.75)3d(0.02)
	N	-0.969	[core]2S (1.41)2p(4.54)3p(0.01)
	C	0.140	[core]2S (0.88)2p(2.96)3p(0.01)
	H	0.436	1S (0.56)

Table 4. (Continued)

Systems	Atom	Natural charge	Natural electron configuration
AMD/C <sub>59</sub> Ga	C	0.001	[core]2S (0.87)2p(3.12)3p(0.01)
	Ga	0.140	[core]4S (0.67)4p(0.93)4d(0.01)
	N	-0.911	[core]2S (1.40)2p(4.49)3p(0.01)
	C	0.140	[core]2S (0.88)2p(2.96)3p(0.01)
	H	0.434	1S (0.56)
AMD/C <sub>59</sub> N	C	0.001	[core]2S (0.87)2p(3.12)3p(0.01)
	N	-0.352	[core]2S (1.42)2p(4.45)3p(0.01)3d (0.01)
	N	-0.886	[core]2S (1.18)2p(4.16)3p(0.01)
	C	0.136	[core]2S (0.87)2p(2.98)3p(0.01)3d (0.01)
AMD/C <sub>59</sub> P	H	0.369	1S (0.63)
	C	0.001	[core]2S (0.87)2p(3.12)3p(0.01)
	P	0.994	[core]3S (1.38)3p(2.58)3d(0.03)4p (0.02)
	N	-0.887	[core]2S (1.41)2p(4.46)3p(0.01)3d (0.01)
AMD/C <sub>59</sub> As	C	0.136	[core]2S (0.87)2p(2.98)3p(0.01)3d (0.01)
	H	0.371	1S (0.63)
	C	0.001	[core]2S (0.87)2p(3.12)3p(0.01)
	As	1.013	[core]4S (1.51)4p(2.46)4d(0.01)5p (0.01)
	N	-0.883	[core]2S (1.42)2p(4.45)3p(0.01)3d (0.01)
	C	0.135	[core]2S (0.87)2p(2.98)3p(0.01)3d (0.01)
H			
	H	0.369	1S(0.63)

for open-shell systems), and the off-diagonal NBO Fock matrix element is demonstrated by  $F(i,j)$ , and  $\Delta E_{ij}^2$  is the stabilization energy.

The results of electron donor–acceptor electron configuration of C<sub>60</sub> and C<sub>59</sub>X are reported in Table 5. It is noteworthy that in this table the most important interactions in terms of the electron transfer stability energy are reported. The existence of such interactions with the remarkable stability energies in this table shows that in all cases the doped atom has been incorporated into the fullerene structure by the chemical interaction and the stability structure has been achieved. In other words, the inserted atom behaves as a doping atom. The data in Table 5 show that the most important interaction for the pristine C<sub>60</sub> related to electron transfer from the BD (C–C) bond as the electron donor to the BD\*(N–H) as the receptor. This is in agreement with the results of the absorption energy as well as with the other results which have examined. In the study of the doped complexes, it is observed that in the X-doped complex, the X atom electron pair is an electron donor (Lewis base) and the

**Table 5. Acceptor NBO interactions and second-order perturbation energies ( $E(2)$ ) for the AMD clusters with pristine C<sub>60</sub> and C<sub>59</sub>X ( $X = Si, Ge, B, Al, Ga, N, P, and As$ ). All values obtained from completed fullerenes at the B3LYP-D3/6-311G (d) level of theory.**

Systems	Donor NBO (i)	Acceptor NBO (j)	E2(kcal/mol)
AMD/C <sub>60</sub>	BD (C–H)	BD*(C–C)	0.06
	BD (N–H)	BD*(C–C)	0.05
	BD (N–H)	BD*(C)	0.06
	BD (C–C)	LP*(Si)	1.01
	BD (C–N)	LP*(Si)	10.56
	BD (C–H)	LP*(Si)	0.07
AMD/C <sub>59</sub> Si	BD (C–H)	BD*(C–Si)	0.78
	BD (C–H)	BD*(C–C)	0.27
	BD (N–H)	LP*(Si)	13.2
	BD (N–H)	BD*(C–Si)	1.34
	BD (N–H)	RY*(C)	0.11
	BD (C–C)	RY*(Ge)	0.06
AMD/C <sub>59</sub> Ge	BD (C–C)	LP*(Ge)	0.79
	BD (C–C)	RY*(C)	0.06
	BD (C–H)	RY*(C)	0.19
	BD (C–H)	RY*(Ge)	0.79
	BD (C–H)	LP*(Ge)	0.79
	BD (C–H)	BD*(C–Ge)	0.96
AMD/C <sub>59</sub> B	BD (C–N)	RY*(Ge)	0.14
	BD (C–N)	RY*(C)	0.07
	BD (C–N)	BD*(C–Ge)	0.09
	BD (N–H)	RY*(Ge)	11.14
	BD (N–H)	LP*(Ge)	0.33
	BD (N–H)	RY*(C)	0.17
AMD/C <sub>59</sub> Al	BD (N–H)	BD*(C–Ge)	1.49
	BD (C–H)	BD*(C–C)	0.03
	BD (N–H)	BD*(C–C)	0.04
	BD (C–H)	RY*(C)	0.04
	BD (C–H)	BD*(C–C)	0.04
	BD (C–N)	RY*(C)	0.03
AMD/C <sub>59</sub> Ga	BD (N–H)	RY*(C)	0.06
	BD (C–C)	LP*(Ga)	0.64
	BD (C–C)	BD*(C–Ga)	0.04
	BD (C–C)	RY*(Ga)	0.03
	BD (C–H)	LP*(Ga)	0.28
	BD (C–H)	BD*(C–Ga)	0.11
AMD/C <sub>59</sub> N	BD (C–H)	RY*(C)	0.03
	BD (C–H)	BD*(C–C)	0.12
	BD (C–N)	LP*(Ga)	4.21
	BD (C–N)	BD*(C–Ga)	0.16
	BD (C–N)	RY*(Ga)	0.15
	BD (N–H)	LP*(Ga)	5.23
AMD/C <sub>59</sub> P	BD (N–H)	BD*(C–Ga)	0.45
	BD (N–H)	RY*(Ga)	0.14
	BD (C–C)	BD*(C–H)	0.19
	BD (C–H)	BD*(C–P)	0.06
	BD (N–H)	BD*(C–P)	0.03
AMD/C <sub>59</sub> As	BD (C–C)	BD*(C–As)	0.03
	BD (C–H)	BD*(C–As)	0.8
	BD (C–H)	RY*(As)	0.04

N-bonded electron pair is the AMD group is electron acceptor (Lewis acid). The highest electron–acceptor stabilization energy in all cases is due to the same interaction, which indicates strong adsorption of the molecule onto the C<sub>59</sub>Ga fullerene compared to the others.

### 3.4. QTAIM analysis

The QTAIM method proposed by Bader *et al.*<sup>76–81</sup> According to this theory, the critical point of the electron density, which can be a minimum point, a maximum point, or a saddle point, can fall into one of the following four categories: (1) *Atomic critical point* (ACP), (2) *bond critical point* (BCP), (3) *ring critical point* (RCP), and (4) *cage critical point* (CCP). The Poincaré–Hopf relationship should be satisfied to verify if all CPs may have been found as follows<sup>82,83</sup>:

The eigenvalues of Hessian matrix,  $\lambda_1$ , and  $\lambda_2$ , are negative and  $|\lambda_1| < |\lambda_2|$  for the BCP. The  $\rho(r)$  and  $\nabla^2\rho(r)$  play an important role in the segmentation and identification of different types of chemical interactions. A BCP with negative values of  $\nabla^2\rho(r)$  and large values of  $\rho(r)$  (of orders exceeding 10–1 a.u.) is defined as a shared (covalent) intermolecular interaction. Also, when  $\nabla^2\rho(r)$  is positive, the interactions can be classified as of the nonsubstrate close-shell type (which includes ionic and van der Waals interactions).<sup>84</sup> The elliptical bond ( $\varepsilon$ ).<sup>85</sup> and the virial theorem<sup>86</sup> are two other important factors in the classification of bonds. An elliptical bond represents the electron density preferentially accumulated on a plate containing the bond and is defined as follows:

$$\varepsilon = \frac{\lambda_1}{\lambda_2} - 1 \quad \text{where} \quad |\lambda_1| > |\lambda_2|. \quad (21)$$

Large values of  $\varepsilon$  indicate an unstable structure and vice versa. Also, based on the virial theorem, the following relationship exists between the electron kinetic energy density  $G(r)$ ,<sup>87</sup> the electron potential energy density  $V(r)$ <sup>88</sup> and  $\nabla^2\rho(r)$ :

$$\frac{1}{4}\nabla^2\rho(r) = 2G(r) + V(r). \quad (22)$$

The balance between  $G(r)$  and  $V(r)$  reflects the nature of the interaction. If  $G/|V|$  ratio is less than 0.5, the nature of the interaction will be purely covalent, and if this ratio is greater than 1, the interaction may be considered as completely noncovalent. Note that for covalent bonds (i.e.  $\nabla^2\rho(r) < 0$  and  $G/|V| < 0.5$ ), the nature of the bond from van der Waals interactions to strong covalent interactions becomes covalent. It can

also play a decisive role in controlling the amount of ionic interaction for closed-shell interactions (i.e.  $\nabla^2\rho(r) > 0$  and  $G/|V| > 1$ ), as they become stronger ionically (and weakly electrostatic) by reducing interactions. Therefore, the QTAIM topology analysis together with WBI analysis and adsorption results exposes an important trend: by increasing the ionic character of atomic bonds in the fullerene, the tendency of the AMD to adsorb is also increased.

Considerable results can be obtained from reviewing Table S3. It is observed that in all adsorption sites Laplacian of electron energy density has a positive value, i.e. the bond is noncovalent. In the study of doped systems, we found that for all clusters, the energy density and the energy density of Laplacian are high indicating that there is a strong bond between the fullerenes and the AMD molecule and the elliptical bond is close to 0, which means the interaction is strong. As stated above, the ratio  $G/|V|$  more than 1 means noncovalent bonding, in the case of Si, Ge, Al, and Ga-doped clusters these amounts are less than 1. In other words, the results of QTAIM analysis also confirm the strong adsorption of the AMD molecule on the C<sub>59</sub>Al and C<sub>59</sub>Ga (see Fig. 7).

The reduced density gradient (RDG) function as well as  $\text{sign}\lambda_2(r)\rho(r)$  function are used to evaluate the weak interactions. These functions are categorized in the context of noncovalent interaction methods which is a powerful way to analyze the types of intermolecular interactions. The RDG is defined as follows<sup>89,90</sup>:

$$\text{RDGs} = \frac{1}{2(3\pi^2)^{\frac{1}{3}}} \frac{|\overline{\Delta\rho}(r)|}{\rho(r)^{\frac{4}{3}}}. \quad (23)$$

The strength of the interaction has a positive correlation with electron density  $\rho(r)$  and the second largest eigenvalue of the Hessian matrix ( $\lambda_2$ ). Thus, the real space function  $\text{sign}\lambda_2(r)\rho(r)$  (the products of the signs of  $\lambda_2$  and  $\rho$ ) can be defined. The scatter graph of the sign of the  $\lambda_2(r)\rho(r)$  function (X-axis) and RDG (Y-axis) reveals the interaction type between AMD and fullerenes. The RDG values range from medium to very large around the nuclei and edges of the molecules, whereas weak interactions (zero to medium) are observed around the chemical bonds. Also, for each specific value of RDG (seen as a horizontal line on the graph), the regions of the graph can be classified into three types, namely,  $\text{sign}\lambda_2(r)\rho(r) < 0$  (strong attraction),  $\text{sign}\lambda_2(r)\rho(r) \approx 0$  (weak van der Waals interaction), and  $\text{sign}\lambda_2(r)\rho(r) > 0$  (strong repulsion (steric effect in ring)).<sup>89,90</sup>

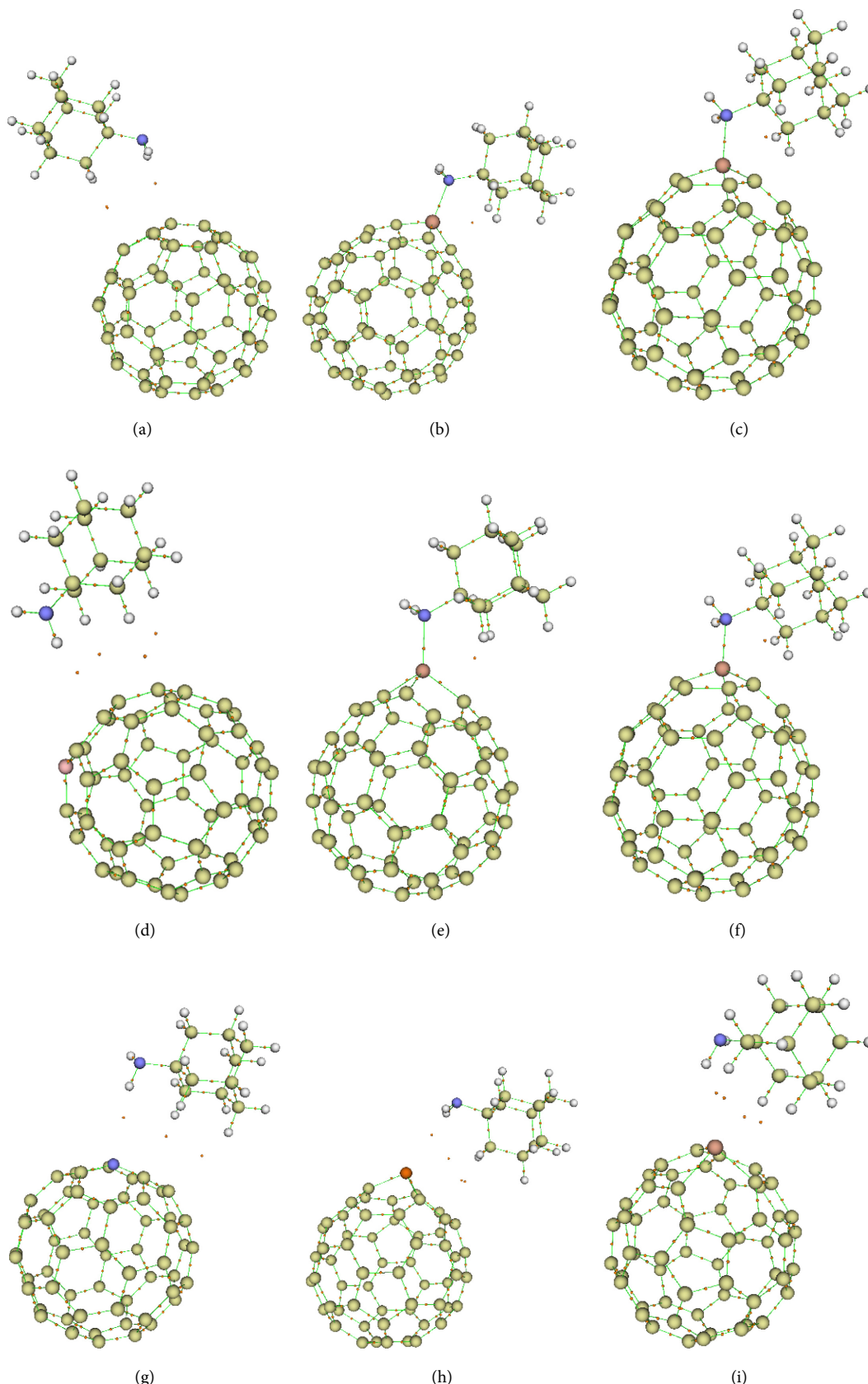


**Fig. 7.** (Color online) QTAIM molecular graphs for the adsorption of AMD onto the surface of (a) C<sub>60</sub>, (b) C<sub>59</sub>Si, (c) C<sub>59</sub>Ge, (d) C<sub>59</sub>B, (e) C<sub>59</sub>Al, (f) C<sub>59</sub>Ga, (g) C<sub>59</sub>N, (h) C<sub>59</sub>P, and (i) C<sub>59</sub>As. Orange dots represent the boundary critical points (BCPs).

Using the isosurface RDG = 0.5 as a reference, it can be concluded that after adsorption of the AMD onto the outer surfaces of the fullerenes, spots appeared around the region characterized by  $\text{sign}\lambda_2(r)\rho(r) \approx 0$ .

The interaction of AMD with fullerenes is in the range of strong van der Waals interactions in nature. Significant changes in the overall features of the pristine  $C_{60}$  graph (Figs. 8 and 9) after the adsorption of AMD were

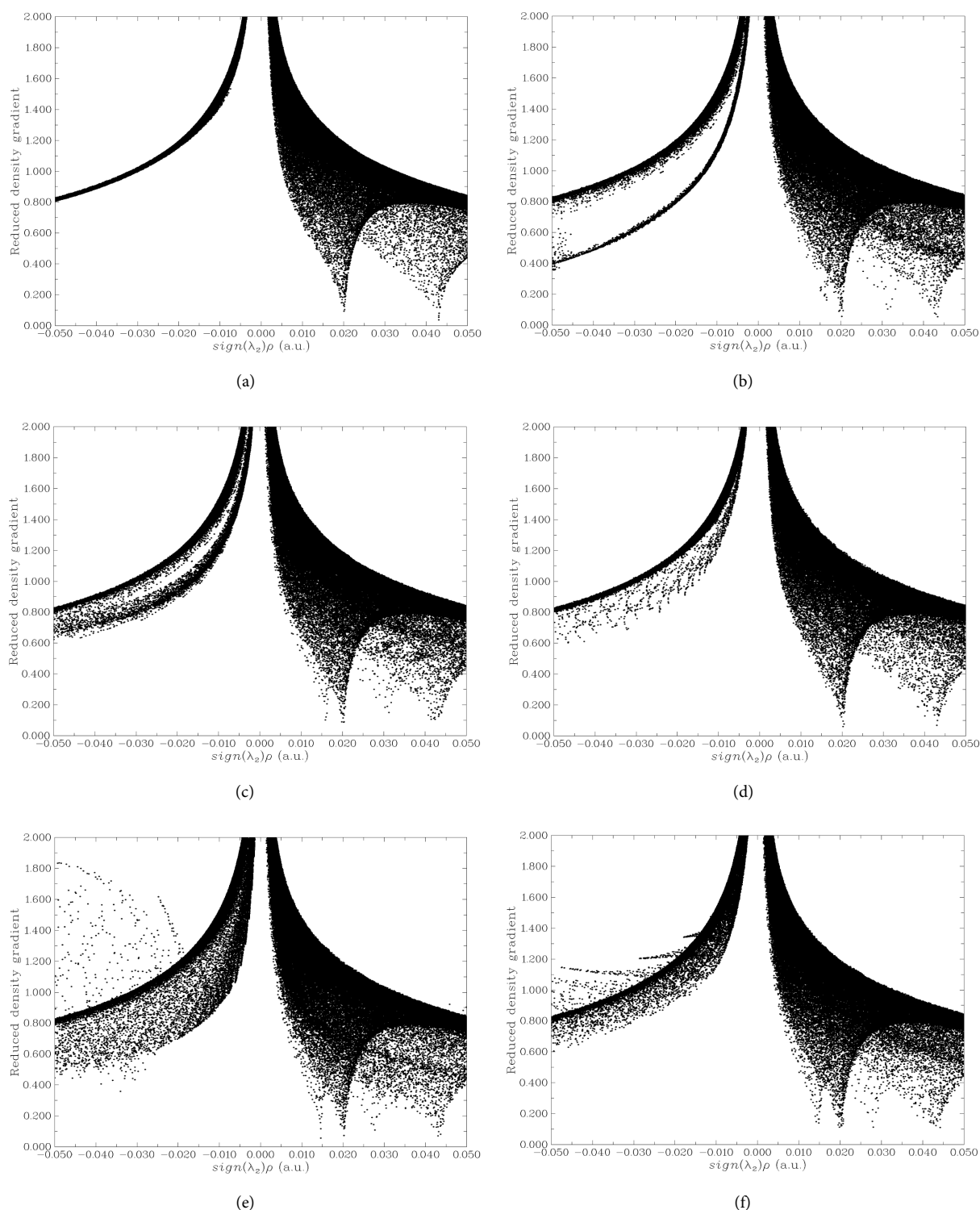


**Fig. 8.** Plots for the average reduced density gradient (aRDG) ( $Y$ -axes) versus  $\text{sign}(\lambda_2)\rho(r)$  ( $X$ -axes) values for (a)  $C_{60}$ , (b)  $C_{59}\text{Si}$ , (c)  $C_{59}\text{Ge}$ , (d)  $C_{59}\text{B}$ , (e)  $C_{59}\text{Al}$ , (f)  $C_{59}\text{Ga}$ , (g)  $C_{59}\text{N}$ , (h)  $C_{59}\text{P}$ , and (i)  $C_{59}\text{As}$ . The data were obtained from B3LYP-D3/6-311G (d) level of theory.

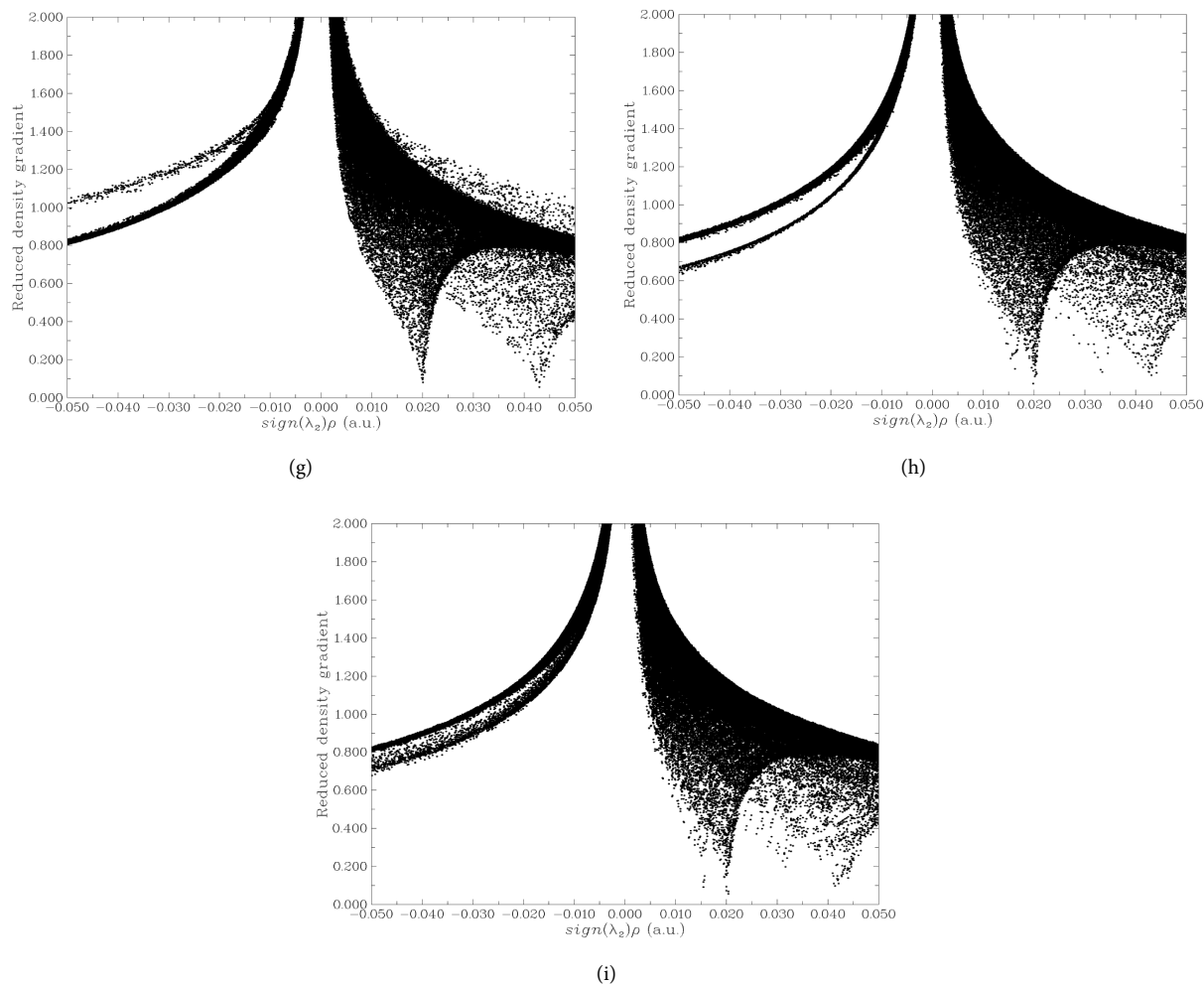
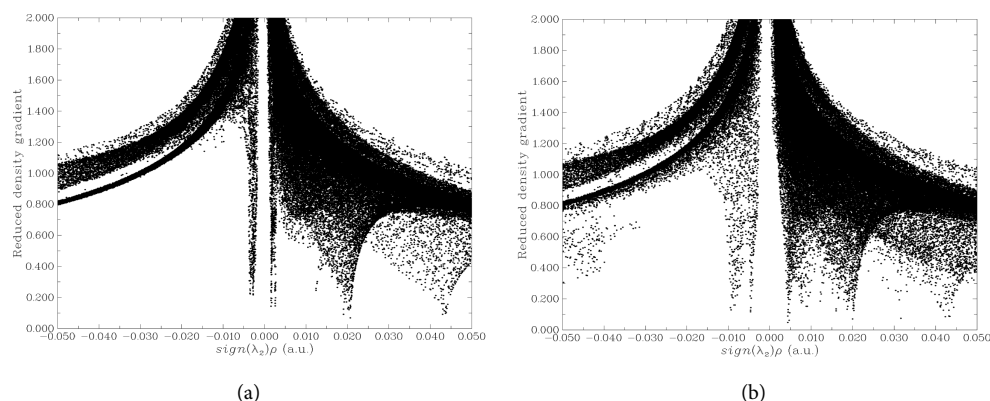


Fig. 8. (Continued)



**Fig. 9.** Plots for the average reduced density gradient (aRDG) (Y-axes) versus  $\text{sign}(\lambda_2)\rho(r)$  (X-axes) values for (a) AMD/C<sub>60</sub>, (b) AMD/C<sub>59</sub>Si, (c) AMD/C<sub>59</sub>Ge, (d) AMD/C<sub>59</sub>B, (e) AMD/C<sub>59</sub>Al, (f) AMD/C<sub>59</sub>Ga, (g) AMD/C<sub>59</sub>N, (h) AMD/C<sub>59</sub>P, and (AMD/i) C<sub>59</sub>As. The data were obtained from B3LYP-D3/6-311G (d) level of theory.

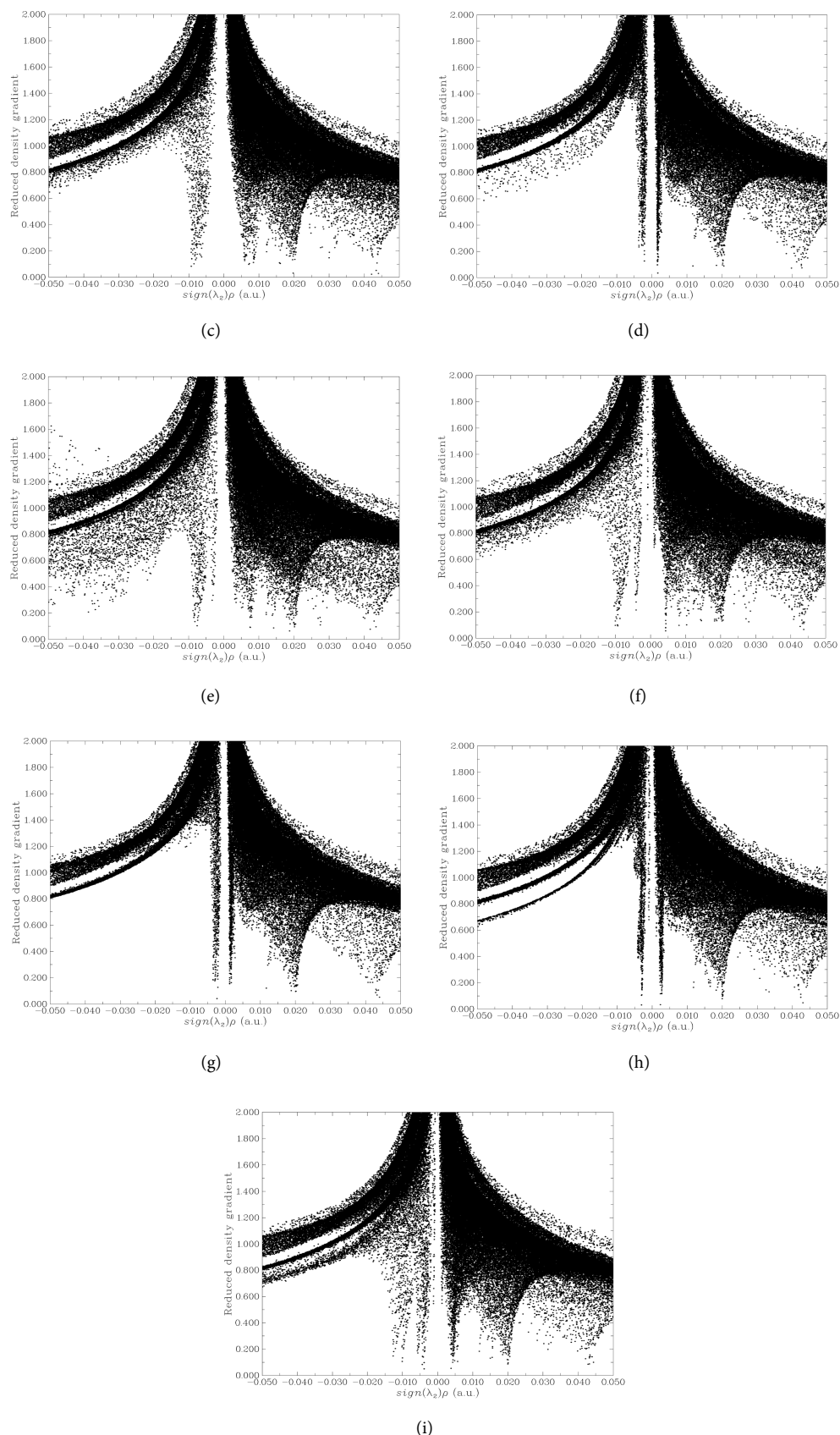


Fig. 9. (Continued)

observed in the region characterized as  $\text{sign}\lambda_2(r)\rho(r) < 0$  (i.e. strong attraction), implying that the AMD/fullerene interactions were strong. Hence, this analysis also confirms the results of the single-point energy calculations and NBO analysis, namely that the interactions of AMD with  $C_{59}X$  were strong.

#### 4. CONCLUSION

In this study, the interactions between AMD molecule and pristine ( $C_{60}$ ) and  $C_{59}X$  ( $X = \text{Si, Ge, B, Al, Ga, N, P, and As}$ ) decorated fullerene were investigated using density functional framework. To this end, the structure of the fullerenes and AMD molecule was optimized at the theoretical level of HSEH1PBE/6-311G (d). Right after that B3LYP-D3, M062X and wB97XD functionals and the same basis set were also used to consider the contribution of long-range interactions and dispersion effect. QTAIM and NBO analyzes were also implemented to consider the character of intermolecular interactions. The results of all analyses are in agreement as follows: (1) Among the different positions studied for pristine silicon carbide fullerene, the  $T_4$  position has the highest absorption energy; (2) investigations in this study show that the Si, Ge, B, Al, Ga, N, P and As elements can be substituted by carbon atom in the fullerene by chemical bonding and, as a binding element, cause dramatic changes in the chemical, electronic and mechanical structure of  $C_{60}$ ; (3) Among the doped structures, Ge-doped system has very high adsorption energy compared to other elements, and is expected to be chemically adsorbed in this case and appears to be a suitable drug carrier characteristic option. The next category is the Al element, where the adsorption energy is higher than the initial state but lower than that of Ga. Generally, we found that the adsorption tendencies of the AMD molecule have a positive correlation to the nature of the bonds in  $C_{60}$  and  $C_{59}X$  structures. Finally, we conclude that the  $C_{60}$  and  $C_{59}X$  are favorable candidates for utilization as a drug carrier vehicle to move AMD molecule.

#### ACKNOWLEDGMENT

I would like to thank the Solid-State Theory Group at the Physics Department at the Universita' degli Studi di Milano-Italy for providing computational facilities.

#### References

- Kroto, H. W.; Heath, J. R.; O'Brien, S. C.; Curl, R. F.; Smalley, R. E. *Nature*, **1985**, 318 (6042), 162–163.
- Iijima, S. *Nature*, **1991**, 354 (6348), 56–58.
- Buseck, P. R.; Tsipursky, S. J.; Hettich, R. *Science*, **1992**, 257 (5067), 215–217.
- Rouse, J. G.; Yang, J.; Ryman-Rasmussen, J. P.; Barron, A. R.; Monteiro-Riviere, N. A. *Nano Lett.* **2007**, 7 (1), 155–160.
- Wang, Q.; Wang, C.; Wang, Z.; Zhang, J.; He, D. *Appl. Phys. Lett.* **2007**, 91 (14), 141902.
- Yakobson, B.; Samsonidze, G.; Samsonidze, G. *Carbon*, **2000**, 38 (11–12), 1675–1680.
- Yakobson, B. I.; Smalley, R. E. *Amer. Sci.* **1997**, 85 (4), 324–337.
- Erb, T.; Zhokhavets, U.; Gobsch, G.; Raleva, S.; Stühn, B.; Schilinsky, P.; Waldauf, C.; Brabec, C. *J. Adv. Funct. Mater.* **2005**, 15 (7), 1193–1196.
- Kataura, H.; Maniwa, Y.; Abe, M.; Fujiwara, A.; Kodama, T.; Kikuchi, K.; Imahori, H.; Misaki, Y.; Suzuki, S.; Achiba, Y. *Appl. Phys. A* **2002**, 74 (3), 349–354.
- Kolodney, E.; Tsipinyuk, B.; Budrevich, A. *J. Chem. Phys.* **1994**, 100 (11), 8542–8545.
- Omri, N.; Oualha, M. A.; Vahabi, H.; Amdouni, N.; Abderrabba, M.; Laoutid, F. *Thermochim. Acta* **2018**, 668, 73–79.
- Stetzer, M.; Heiney, P.; Fischer, J.; McGhie, A. *Phys. Rev. B* **1997**, 55 (1), 127.
- Goyal, R. N.; Singh, S. P. *Talanta*, **2006**, 69 (4), 932–937.
- Lian, Z.; Xu, P.; Wang, W.; Zhang, D.; Xiao, S.; Li, X.; Li, G. *ACS Appl. Mater. Interf.* **2015**, 7 (8), 4533–4540.
- Yildirim, T.; Íñiguez, J.; Ciraci, S. *Phys. Rev. B* **2005**, 72 (15), 153403.
- Ruoff, R.; Tse, D. S.; Malhotra, R.; Lorents, D. C. *J. Phys. Chem.* **1993**, 97 (13), 3379–3383.
- Ahmadi, R.; Salmaniha, M. *Int. J. New Chem.* **2014**, 1 (4), 151–159.
- Wu, H.; Fan, X.; Kuo, J.-L. *Int. J. Hydrogen Energy* **2012**, 37 (19), 14336–14342.
- Charkin, O.; Klimenko, N.; Charkin, D. *Adv. Quantum Chem.* **2009**, 58, 69–114.
- Zheng, G.; Irle, S.; Morokuma, K. *Chem. Phys. Lett.* **2005**, 412 (1–3), 210–216.
- Xie, R.-H.; Bryant, G. W.; Sun, G.; Nicklaus, M. C.; Heringer, D.; Frauenheim, T.; Manaa, M. R.; Smith Jr, V. H.; Araki, Y.; Ito, O. *J. Chem. Phys.* **2004**, 120 (11), 5133–5147.
- Matsubara, M.; Massobrio, C. *J. Phys. Chem. A* **2005**, 109 (19), 4415–4418.
- Haddon, R. *Accounts Chem. Res.* **1992**, 25 (3), 127–133.
- Parlak, C.; Alver, O.; Şenyel, M. *J. Theor. Comput. Chem.* **2017**, 16 (2), 1750011.
- Chandrakumar, K.; Ghosh, S. K. *Nano Lett.* **2008**, 8 (1), 13–19.
- El Mahdy, A. *Appl. Surf. Sci.* **2016**, 383, 353–366.
- Gökpek, Y.; Bilge, M.; Bilge, D.; Alver, O.; Parlak, C. *J. Mol. Liq.* **2017**, 238, 225–228.
- Hazrati, M. K.; Hadipour, N. L. *Phys. Lett. A* **2016**, 380 (7–8), 937–941.

29. Hobbs, C.; Kantorovich, L.; Gale, J. D. *Surf. Sci.* **2005**, *591* (1–3), 45–55.
30. Shariatinia, Z.; Shahidi, S. *J. Mol. Graph. Model.* **2014**, *52*, 71–81.
31. Parlak, C.; Alver, O. {\hskip 3pt \vskip 2pt.} *Chem. Phys. Lett.* **2017**, *678*, 85–90.
32. Davies, W.; Grunert, R.; Haff, R.; McGahen, J.; Neu-mayer, E.; Paulshock, M.; Watts, J.; Wood, T.; Hermann, E.; Hoffmann, C. *Science*, **1964**, *144* (3620), 862–863.
33. Mucke, H. *Drug Repositioning: Approaches and Applications for Neurotherapeutics*, CRC Press, **2017**.
34. Hubsher, G.; Haider, M.; Okun, M. *Neurology*, **2012**, *78* (14), 1096–1099.
35. Hounshell, D. A.; Smith, J. *Science and Corporate Strategy: Du Pont R&D, 1902–1980*, Cambridge University Press, Cambridge, **2006**.
36. Maugh, T. H. *Science*, **1979**, *206* (4422), 1058–1060.
37. Vollum, D. I.; Parkes, J.; Doyle, D. *Br. Med. J.* **1971**, *2* (5762), 627–628.
38. Patra, B.; Ghosh, P.; Das, S. P. *Drosophila melanogaster: A model organism to understand biological activities of nanoparticles*, in *Model Organisms to Study Biological Activities and Toxicity of Nanoparticles*, Springer, **2020**, pp. 195–216.
39. Ahmadi, R. *J. Phys. Theor. Chem.* **2012**, *9* (3), 185–190.
40. Hehre, W. J.; Ditchfield, R.; Pople, J. A. *J. Chem. Phys.* **1972**, *56* (5), 2257–2261.
41. M. J. Frisch, G. W. Trucks, H. B. Schlegel, G. E. Scuseria, M. A. Robb, J. R. Cheeseman, G. Scalmani, V. Barone, G. A. Petersson, H. Nakatsuji, X. Li, M. Caricato, A. V. Marenich, J. Bloino, B. G. Janesko, R. Gomperts, B. Mennucci, H. P. Hratchian, J. V. Ortiz, A. F. Izmaylov, J. L. Sonnenberg, Williams, F. Ding, F. Lipparini, F. Egidi, J. Goings, B. Peng, A. Petrone, T. Henderson, D. Ranasinghe, V. G. Zakrzewski, J. Gao, N. Rega, G. Zheng, W. Liang, M. Hada, M. Ehara, K. Toyota, R. Fukuda, J. Hasegawa, M. Ishida, T. Nakajima, Y. Honda, O. Kitao, H. Nakai, T. Vreven, K. Throssell, J. A. Montgomery Jr., J. E. Peralta, F. Ogliaro, M. J. Bearpark, J. J. Heyd, E. N. Brothers, K. N. Kudin, V. N. Staroverov, T. A. Keith, R. Kobayashi, J. Normand, K. Raghavachari, A. P. Rendell, J. C. Burant, S. S. Iyengar, J. Tomasi, M. Cossi, J. M. Millam, M. Klene, C. Adamo, R. Cammi, J. W. Ochterski, R. L. Martin, K. Morokuma, O. Farkas, J. B. Foresman, D. J. Fox, Gaussian 16 Rev. C.01, Wallingford, CT, 2016.
42. Lu, T.; Chen, F. *J. Comput. Chem.* **2012**, *33* (5), 580–592.
43. Lu, T.; Chen, F. *J. Mol. Graph. Model.* **2012**, *38*, 314–323.
44. Lu, T.; Chen, Q. *Theor. Chem. Accounts* **2020**, *139* (2), 25.
45. J. B. Foresman, A. Frisch, Exploring chemistry with electronic structure methods: A guide to using Gaussian, (1996).
46. Parr, R. G.; Donnelly, R. A.; Levy, M.; Palke, W. E. *J. Chem. Phys.* **1978**, *68* (8), 3801–3807.
47. von Szentpály, L. *J. Phys. Chem. A* **1998**, *102* (52), 10912–10915.
48. Janak, J. *Phys. Rev. B* **1978**, *18* (12), 7165.
49. Parr, R. G. Density functional theory of atoms and molecules, in *Horizons of Quantum Chemistry*, Springer (1980), pp. 5–15.
50. P. Chattaraj, D. Roy, Electrophilicity Index, *Chem. Rev.* **2006**, *106* (6) 2065; Update 1 of: Electrophilicity Index, *Chem. Rev.* **2007**, *107* (9) PR46–PR74.
51. Parr, R. G.; Szentpaly, L. V.; Liu, S. *J. Am. Chem. Soc.* **1999**, *121* (9), 1922–1924.
52. Noorizadeh, S.; Maihami, H. *J. Mol. Struct. Theochem* **2006**, *763* (1–3), 133–144.
53. Weinhold, F. *Discovering Chemistry with Natural Bond Orbitals*, John Wiley & Sons, 2012.
54. Weinhold, F.; Landis, C. R. *Valency and Bonding: A Natural Bond Orbital Donor-Acceptor Perspective*, Cambridge University Press, **2005**.
55. Carpenter, J.; Weinhold, F. *J. Mol. Struct. THEOCHEM* **1988**, *169*, 41–62.
56. Foster, A. J., Weinhold, F. *J. Am. Chem. Soc.* **1980**, *102* (24), 7211–7218.
57. Glendening, E., Badenhoop, J., Reed, A., Carpenter, J., Bohmann, J., Morales, C., Landis, C., Weinhold, F. Theoretical Chemistry Institute, University of Wisconsin, Madison, 2013.
58. Reed, A. E.; Weinhold, F. *J. Chem. Phys.* **1983**, *78* (6), 4066–4073.
59. Reed, A. E.; Weinhold, F. *J. Chem. Phys.* **1985**, *83* (4), 1736–1740.
60. Reed, A. E.; Weinstock, R. B.; Weinhold, F. *J. Chem. Phys.* **1985**, *83* (2), 735–746.
61. Glendening, E. D.; Landis, C. R.; Weinhold, F. *Wiley Interdiscip. Rev. Comput. Mol. Sci.* **2012**, *2* (1), 1–42.
62. Glendening, E. D.; Landis, C. R.; Weinhold, F. *J. Comput. Chem.* **2019**, *40* (25), 2234–2241.
63. Reed, A. E.; Curtiss, L. A.; Weinhold, F. *Chem. Rev.* **1988**, *88* (6), 899–926.
64. Weinhold, F. Natural bond orbital methods, *Encyclopedia Comput. Chem.* **2002**, 3.
65. Weinhold, F. *J. Comput. Chem.* **2012**, *33* (30), 2363–2379.
66. Weinhold, F.; Landis, C.; Glendening, E. *Int. Rev. Phys. Chem.* **2016**, *35* (3), 399–440.
67. Mulliken, R. S. *J. Chem. Phys.* **1955**, *23* (10), 1833–1840.
68. Mayer, I. *Chem. Phys. Lett.* **1983**, *97* (3), 270–274.
69. Mayer, I. *Chem. Phys. Lett.* **2012**, *544*, 83–86.
70. Giambiagi, M.; de Giambiagi, M. S.; Mundim, K. C. *Struct. Chem.* **1990**, *1* (5), 423–427.
71. Matito, E. *Phys. Chem. Chem. Phys.* **2016**, *18* (17), 11839–11846.
72. Wiberg, K. B. *Tetrahedron* **1968**, *24* (3), 1083–1096.
73. Lu, T.; Chen, F. *J. Phys. Chem. A* **2013**, *117* (14), 3100–3108.
74. Mayer, I.; Salvador, P. *Chem. Phys. Lett.* **2004**, *383* (3–4), 368–375.

75. Sizova, O. V.; Skripnikov, L. V.; Sokolov, A. Y. *J. Mol. Struct. Theochem.* **2008**, *870* (1–3), 1–9.
76. Bader, R.; Nguyen-Dang, T. T.; Tal, Y. *Rep. Prog. Phys.* **1981**, *44* (8), 893.
77. Bader, R. F. *Accounts Chem. Res.* **1985**, *18* (1), 9–15.
78. Bader, R. F. *Chem. Rev.* **1991**, *91* (5), 893–928.
79. Bader, R. F.; Matta, C. F. *Found. Chem.* **2013**, *15* (3), 253–276.
80. Biegler-könig, F. W.; Bader, R. F.; Tang, T. H. *J. Comput. Chem.* **1982**, *3* (3), 317–328.
81. Cortés-Guzmán, F.; Bader, R. F. *Coord. Chem. Rev.* **2005**, *249* (5–6), 633–662.
82. Balanarayan, P.; Gadre, S. R. *J. Chem. Phys.* **2003**, *119* (10), 5037–5043.
83. Roy, D.; Balanarayan, P.; Gadre, S. R. *J. Chem. Phys.* **2008**, *129* (17), 174103.
84. Matta, C. F., Hydrogen–hydrogen bonding: The non-electrostatic limit of closed-shell interaction between two hydro, in *Hydrogen Bonding—New Insights*, Springer, pp. 337–375, **2006**.
85. Bohórquez, H. J.; Boyd, R. J.; Matta, C. F. *J. Phys. Chem. A* **2011**, *115* (45), 12991–12997.
86. Grabowski, S. J. *J. Phys. Chem. A* **2012**, *116* (7), 1838–1845.
87. Tal, Y.; Bader, R. *Int. J. Quantum Chem.* **1978**, *14* (S12), 153–168.
88. Keith, T.; Bader, R.; Aray, Y. *Int. J. Quantum Chem.* **1996**, *57* (2), 183–198.
89. Contreras-García, J.; Johnson, E. R.; Keinan, S.; Chaudret, R.; Piquemal, J.-P.; Beratan, D. N.; Yang, W. *J. Chem. Theory Comput.* **2011**, *7* (3), 625–632.
90. Johnson, E. R.; Keinan, S.; Mori-Sánchez, P.; Contreras-García, J.; Cohen, A. J.; Yang, W. *J. Am. Chem. Soc.* **2010**, *132* (18), 6498–6506.